Exosomes derived from human dermal fibroblasts protect against UVB-induced skin photoaging

A YEON PARK[1,2*], JUNG OK LEE[1,2*], YOUNA JANG[1], YU-JIN KIM[1,2], JUNG MIN LEE[1], SU-YOUNG KIM[1,2], BEOM JOON KIM[1,2] and KWANG HO YOO[3]

[1]Department of Dermatology, College of Medicine, Chung-Ang University; [2]Department of Medicine, Graduate School, Chung-Ang University, Seoul 06974; [3]Department of Dermatology, Chung-Ang University Gwang-Myeong Hospital, Chung-Ang University College of Medicine, Gwangmyeong-si, Gyeonggi-do 14353, Republic of Korea

Received May 3, 2023; Accepted September 27, 2023

DOI: 10.3892/ijmm.2023.5323

Abstract. Exosomes are used as innovative treatment options for repairing skin defects, such as aging, atopic dermatitis and wounds. However, the effects of exosomes obtained from human foreskin fibroblasts BJ-5ta (BJ-5ta Exo) on ultraviolet B (UVB)-mediated photoaging have not been previously reported, at least to the best of our knowledge. Therefore, the present study aimed to investigate the anti-photoaging effects of BJ-5ta Exo on UVB radiation in human skin fibroblasts and SKH-1 hairless mice. The results revealed that BJ-5ta Exo decreased the production of reactive oxygen species and inhibited the decrease in the expression levels of superoxide dismutase 1 and 2, glutathione peroxidase and catalase following UVB exposure. In addition, BJ-5ta Exo attenuated the decrease in nuclear factor erythroid 2-related factor 2 levels induced by UVB rays, indicating its scavenging activity against oxidative stress. Moreover, BJ-5ta Exo inhibited the UVB-induced increase in the levels of γH2AX, p53/21 and cleaved PARP, whereas it promoted DNA double-strand break repair through radiation sensitive 52 and effectively activated the TGF-β1/Smad pathway. BJ-5ta Exo also protected against UVB-induced senescence, as indicated by the downregulation in the levels of senescence-associated β-galactosidase and p16. In a mouse model of photoaging, BJ-5ta Exo prevented the UVB-induced increase in transepidermal water loss, wrinkle formation and MMP-1 expression, while also suppressing the UVB-mediated decrease in collagen type I and elastin levels in the dorsal skin. Overall, the findings of the present study suggest that BJ-5ta Exo represent an effective anti-photoaging agent, which can be used as a component in cosmetic products.

Correspondence to: Professor Kwang Ho Yoo, Department of Dermatology, Chung-Ang University Gwang-Myeong Hospital, Chung-Ang University College of Medicine, 110 Deokan-ro, Gwangmyeong-si, Gyeonggi-do 14353, Republic of Korea
E-mail: psyfan9077@naver.com

Professor Beom Joon Kim, Department of Dermatology, College of Medicine, Chung-Ang University Hospital, 102 Heukseok-ro, Dongjak-gu, Seoul 06974, Republic of Korea
E-mail: beomjoon74@gmail.com

*Contributed equally

Key words: exosome, oxidative stress, DNA damage, ROS, UVB, skin photoaging, BJ-5ta fibroblast

Introduction

Ultraviolet radiation (UVR) poses the greatest threat to the skin as external component. UVR in composed of three wavelength ranges: UVA (320-400 nm), UVB (290-320 nm) and UVC (200-290 nm) (1). Different UVR wavelengths cause skin damage through various mechanisms. UVA exhibits a strong ability to penetrate the skin, reaching the epidermis, dermis and even subcutaneous tissue. On the other hand, the penetrative ability of UVB is weaker, mainly damaging the epidermis and superficial dermis (2-4). However, as the energy of UVR decreases with increasing wavelength, UVB has a stronger detrimental impact on the epidermis compared to UVA (5). Additionally, UVB radiation indirectly stimulates higher levels of epidermal melanin, which serves to protect the skin against DNA damage (6,7).

Repetitive exposure to UVB increases the levels of cellular reactive oxygen species (ROS), which can promote carcinogenesis, cell senescence and other skin pathologies (8-10). Excessive levels of ROS upregulate the production of matrix metalloproteinases (MMPs), which can degrade extracellular matrix components and inhibit collagen synthesis, causing skin relaxation, wrinkles and erythema (11). The skin possesses various protective mechanisms against UVB-induced oxidative damage, including antioxidants such as catalase (CAT), superoxide dismutase (SOD), glutathione peroxidase (GPX) and reduced glutathione (GSH) (12). However, when ROS levels surpass the capacity of these antioxidant defenses, excessive ROS accumulation can disrupt the balance of the oxidation/antioxidant system, leading to DNA damage and cell cycle arrest (13). Given the crucial role of ROS in photoaging, reducing ROS accumulation presents a potential approach for safeguarding the skin against photo-damage.

UVB-mediated DNA damage activates multiple cell signaling pathways related to cell growth, apoptosis, senescence, DNA damage repair, connective tissue degradation and inflammation (14,15). Histone H2AX plays a central role in several repair mechanisms (16,17) and its phosphorylation is associated with DNA double-strand breaks (DSBs). The phosphorylated form of H2AX (Ser^{139}), known as γH2AX, leads to changes in chromatin structure and facilitates the recruitment of DNA repair factors, including p53-binding protein 1, Nijmegen breakage syndrome 1, breast cancer type 1 susceptibility protein, radiation sensitive 52 (RAD52) and mediator of DNA damage checkpoint 1 (18).

Exosomes, which are nanoscale extracellular vesicles, are secreted by all living cells (19). They transfer functional cargo, such as bioactive proteins, messenger ribonucleic acids (mRNAs) and microRNAs, which can mediate cell responses and regulate some biological processes in target cells (20). For example, exosomes derived from human induced pluripotent stem cells (iPSCs) have been reported to significantly reduce the expression levels of MMP-1/3 and senescence-associated β-galactosidase (SA-β-Gal), while upregulating the expression of collagen type I in human dermal fibroblasts (hDFs) (21). Furthermore, Choi *et al* (22) found that exosomes derived from adipose-derived stem cells (ADSCs) effectively suppressed the overexpression of MMPs, and enhanced the expression of collagen type I and elastin (22).

hDFs are the predominant cell type in the dermis and are responsible for regulating the extracellular matrix (ECM), collagen production and wound healing (23). These cells play critical roles in preventing skin aging, and maintaining the normal structure and functions of the skin (24), rendering them essential for skin regeneration and repair. Previous research has demonstrated that hDFs constitute a useful cell line for studying particular aspects of skin aging as they are easily grown in culture and respond to various age-inducing stimuli (25). Additionally, the foreskin is considered a valuable tissue source because it contains immunotherapeutic molecules (26). However, the anti-photoaging activities of exosomes derived from human neonatal foreskin fibroblast cells have not yet been reported, at least to the best of our knowledge. The present study examined the protective effects of exosomes derived from BJ-5ta cells (BJ-5ta Exo) on UVB-induced photoaging. The data demonstrate that BJ-5ta Exo can protect the skin against UVB-induced photoaging.

Materials and methods

Isolation and characterization of exosomes. Human hTERT-immortalized foreskin fibroblast (BJ-5ta) cells were purchased from ATCC (CRL-4001) and maintained in a 4:1 mixture of DMEM and Medium 199 (WelGENE Inc.), supplemented with 10% fetal bovine serum (FBS; HyClone; Cytiva) and 1% penicillin/streptomycin at 37˚C in a humidified incubator with 5% CO_2. To isolate the exosomes, the cells were incubated in serum-free DMEM. The conditioned medium was then collected and centrifuged at 300 x g for 10 min and 2,000 x g for 20 min at 4˚C, followed by filtration to remove the cells and cellular debris using 0.22-μm filters. The clarified supernatant was collected and concentrated using a sterile-membrane T-series cassette (Pall Life Sciences) with tangential flow filtration using a membrane with a molecular weight cut-off (MWCO) of 100 kDa (Sartorius AG). The mixture was then centrifuged at 100,000 x g for 3 h at 4˚C (Fig. S1). The morphology of the BJ-5ta Exo was imaged using a field-emission scanning electron microscope (FE-SEM; Sigma HD, Carl Zeiss Meditec AG). The size distribution was determined by nanoparticle tracking analysis (NTA) using ZetaView (Particle Metrix). In total, two positive exosome markers, CD63 and ALIX, were used, while Calnexin was used as the negative protein marker.

UVB irradiation. Prior to UVB irradiation, the cells were treated with BJ-5ta Exo at a concentration of 10^4 particles/ml for 6 h in a serum-free 4:1 mixture of DMEM and Medium 199 (WelGENE Inc.). UVB irradiation was performed at 30 mJ/cm^2 for <1 min in a thin layer of phosphate-buffered saline (PBS) using a UVB-emitting system from Biospectra (Vilber Lourmat Sto). Following irradiation, the cells were incubated in serum-free medium, and both the cells and cell supernatants were used for further analysis.

Measuring cell viability. The cells were seeded and cultured in 96-well plates (Corning, Inc.) until they reached a confluency of 90%. The cells were treated with BJ-5ta Exo (0, 10^3, 10^4, 10^5, 10^6 and 10^7 particles/ml) for 24 h or exposed to various doses of UVB radiation (20, 30, and 40 mJ/cm^2), followed by incubation at 37˚C with 5% CO_2 for 24 h. In addition, the cells were treated with BJ-5ta Exo (10^4 particles/ml) for 6 h before being exposed to UVB radiation (30 mJ/cm^2) and then incubated at 37˚C with 5% CO_2 for 24 h. Cell viability was assessed using a WST-8 assay kit (QuantiMax™, Biomax). The absorbance was measured at 450 nm using a microplate spectrophotometer (SpectraMax 340; Moleular Devices, Inc.).

Measurement of intracellular ROS levels. The intracellular production of ROS was measured using the Cellular ROS Detection Assay kit (cat. no. ab113851, Abcam). The cells were pre-treated with various concentrations of BJ-5ta Exo for 6 h, washed with 1X assay buffer (Abcam), and incubated in 20 μM in 2,7-dichlorofluorescin diacetate (DCFDA) solution (Abcam) (100 μl) for 45 min at 37˚C with 5% CO_2 in the dark. Subsequently, the cells were exposed to UVB radiation (30 mJ/cm^2) and incubated in complete medium containing 10% fetal bovine serum (FBS), but lacking phenol red (WelGENE Inc.) for 2 h. The samples were observed using a fluorescence microscope (DMi8, Leica Microsystems GmbH), and fluorescence readings were obtained using a spectrophotometer (SpectraMax 340; Molecular Devices, Inc.) at wavelengths of 485 and 535 nm.

SA-β-Gal staining. SA-β-gal staining was performed according to the instructions provided with the SA-β-gal Staining kit (cat. no. 9860, Cell Signaling Technology, Inc.). After washing with PBS (pH 6.0), the cells were fixed in 4% paraformaldehyde (4% PFA) for 10 min at room temperature (RT) and stained at 37˚C for overnight in a dry incubator without CO_2. The SA-β-gal-positive cells were observed using an optical microscope (DMi8, Leica Microsystems GmbH), and the count was determined by examining 400 cells per dish using the Image Pro Plus (IPP) 6.0 software

(Media Cybernetics, Inc.). The proportions of cells exhibiting SA-β-gal activity are presented as percentages of the total cells count in each dish.

Cell cycle assay. The BJ-5ta fibroblasts were pre-treated with BJ-5ta Exo at a concentration of 10^4 particles/ml for 1 h and then irradiated with UVB at a dose of 30 mJ/cm^2. Following 24 h of incubation at 37˚C with 5% CO_2, the cells were fixed with cold ethanol (70%) and then treated with propidium iodide (PI; MilliporeSigma) and RNase A (Thermo Fisher Scientific, Inc.). The cell cycle was assessed using a BD FAC Symphony A1 flow cytometer (BD Biosciences) and analyzed using FlowJo software v10.

Apoptosis analysis. An Annexin V-FITC apoptosis detection kit (V13241, Invitrogen; Thermo Fisher Scientific, Inc.) was used to determine the number of apoptotic cells. The cells were pre-treated with BJ-5ta Exo at concentrations of 10^4 particles/ml for 1 h and then irradiated with UVB (30 mJ/ cm^2). Following exposure, the cells were incubated for 24 h at 37˚C with 5% CO_2, and then collected and centrifuged at 252 x g for 10 min at RT, washed three times with cold PBS and resuspended in 100 μl binding buffer solution. Finally, the cells were incubated with Annexin V-FITC (5 μl) and PI (5 μl) at room temperature for 15 min in the dark. The fluorescence of the cells was immediately assessed using a flow cytometer (BD Biosciences). In the FACS diagram, the early apoptotic cells and the late apoptotic cells are respectively represented in the lower right quadrant and upper right quadrant. The total apoptotic rates were calculated using the following formula: Total apoptosis rate (%)=early apoptosis rate + late apoptosis rate.

Reverse transcription-quantitative PCR (RT-qPCR). Gallic acid (GA), a phenolic antioxidant found in numerous types of plants, a positive control was used due to its antioxidant activity (27). The BJ-5ta fibroblasts were pre-treated with BJ-5ta Exo or GA at a concentration of 10^4 particles/ml for 6 h and then irradiated with UVB at a dose of 30 mJ/cm^2. Following 1 h of incubation at 37˚C with 5% CO_2, total RNA was extracted using TRIzol reagent (Invitrogen; Thermo Fisher Scientific, Inc.). Single-strand cDNA synthesis was performed using reverse transcription using PrimeScript TM RT Master Mix (Takara Bio, Inc.). The resulting cDNA was subjected to qPCR on a CFX96 thermocycler (Bio-Rad Laboratories, Inc.) using qPCR PreMIX SYBR-Green (Enzynomics). The following thermal cycling conditions were used: PCR initial activation step for 15 min at 95˚C; three-step cycling: Denaturation for 10 sec at 95˚C, annealing for 15 sec at 60˚C, elongation for 30 sec at 72˚C; for 45 cycles. Gene expression levels were calculated as a cycle threshold (Ct) value using the $2^{-\Delta\Delta Cq}$ quantification method and normalized to that of glyceraldehyde-3-phosphate dehydrogenase (GAPDH) (28). The primers used for qPCR are listed in Table I.

Table I. Primer sequences used for RT-qPCR.

Gene	Primer sequence (5' to 3')
Human SOD1	F: CGACAGAAGGAAAGTAATG
	R: TGGATAGAGGATTAAAGTGAGG
Human SOD2	F: GCCCTGGAACCTCACATCAA
	R: GGTACTTCTCCTCGGTGACGTT
Human CAT	F: CGTGCTGAATGAGGAACAGA
	R: AGTCAGGGTGGACCTCAGTG
Human GPX	F: CAACCAGTTTGGGCATCAG
	R: TTCACCTCGCACTTCTCG
Human GAPDH	F: TGGAAATCCCATCACCATCTTC
	R: CGCCCCACTTGATTTTGG

Western blot analysis. Whole protein lysates were extracted from BJ-5ta cells using RIPA buffer (Thermo Fisher Scientific, Inc.), and the protein content was quantified using Bradford reagent (MilliporeSigma). Equal amounts of protein (10 μg) were separated on a 10% SDS-PAGE gel and transferred to nitrocellulose membranes (Cytiva, Amersham, United States), which were then blocked in 5% skim milk in Tris-buffered saline containing 0.1% Tween-20 (TBS-T) for 2 h at RT and probed overnight at 4˚C with primary antibodies listed in Table II. The membranes were then incubated with HRP-conjugated anti-mouse (1:5,000, PI-2000-1, Vector Laboratories, Inc.) or anti-rabbit (1:5,000,PI-1000-1, Vector Laboratories, Inc.) secondary antibodies at room temperature for 1 h. Immunodetection was performed using an Amersham ECL kit (GE Healthcare; Cytiva) according to the manufacturer's protocol. The protein bands were visualized using a ChemiDoc™ MP Imaging System (Bio-Rad Laboratories, Inc.) and analyzed using ImageJ software V1.8.0 (National Institutes of Health).

Immunocytochemistry (ICC). The cells were fixed with 4% PFA for 30 min, washed with PBS, blocked with 3% bovine serum albumin (BSA) and 0.2% Triton X-100 in PBS at RT for 1 h, and incubated overnight at 4˚C with primary antibodies listed in Table II. After washing with PBS, the cells were incubated with anti-rabbit IgG-FITC secondary antibodies (1:3,000, ab6717, Abcam) for 1 h at RT in the dark. The cell nuclei were counterstained with 4˚C counterstained 4',6-diamidino-2-phenylindole (DAPI; cat. no. AR-6501-01, ImmunoBioScience Corp.) at RT for 30 min, and the stained cells were observed using a confocal microscope (LSM 880, Zeiss AG).

Experimental animals and UVB irradiation. Female SKH-1 hairless mice (7 weeks old, 17-22 g) were purchased from Saeron Bio, Inc. The mice were acclimatized for 1 week under the following conditions: A temperature of 23±2˚C, 55±10% humidity, and a 12-h-light/12-h-dark cycle. All animal experiments were conducted in accordance with the principles of laboratory animal care at the National Institutes of Health and with the approval of the Ethics Committee for Laboratory Animals at Chung-Ang University (IACUC no. A2022053). The mice were randomly assigned to four groups (n=6 per group) as follows: Group 1, normal control; group 2, UVB only; group 3, UVB + BJ-5ta Exo 10^6 (particles/ml); and group 4, UVB + BJ-5ta Exo 10^8 (particles/ml). The mice were

Table II. Antibodies used for western blot analysis.

Antibodies	Catalogue number	Company	Dilution
Anti-γH2AX	MA1-2022	Thermo Fisher Scientific, Inc.	1:5,000
Anti-iNOS	PA1-038	Thermo Fisher Scientific, Inc.	1:1,000
Anti-MMP1	PA5-27210	Thermo Fisher Scientific, Inc.	1:5,000
Anti-p53	ab131442	Abcam	1:1,000
Anti-p16	ab81278	Abcam	1:1,000
Anti-collagen type I	ab21965	Abcam	1:1,000
Anti-RAD51	ab176458	Abcam	1:5,000
ALIX	ab275377	Abcam	1:1,000
CD63	ab134045	Abcam	1:1,000
CALNEXIN	Ab22595	Abcam	1:1,000
Anti-p21	2947s	Cell Signaling Technology, Inc.	1:5,000
Anti-β-actin	3700s	Cell Signaling Technology, Inc.	1:5,000
Anti-cleaved PARP	5625s	Cell Signaling Technology, Inc.	1:1,000
Anti-p-NF-κB (Ser^{536})	3033s	Cell Signaling Technology, Inc.	1:1,000
Anti-NF-κB	8242s	Cell Signaling Technology, Inc.	1:1,000
Anti-COX-2	12282s	Cell Signaling Technology, Inc.	1:5,000
Anti-p-p38 (Thr^{180}/Tyr^{182})	4511s	Cell Signaling Technology, Inc.	1:1,000
Anti-p38	9212s	Cell Signaling Technology, Inc.	1:5,000
Anti-p-JNK (Thr^{183}/Tyr^{185})	9251s	Cell Signaling Technology, Inc.	1:5,000
Anti-JNK	9252s	Cell Signaling Technology, Inc.	1:5,000
Anti-p-ERK (Thr^{202}/Tyr^{204})	9101s	Cell Signaling Technology, Inc.	1:5,000
Anti-ERK	9102s	Cell Signaling Technology, Inc.	1:5,000
Anti-p-c-Jun (Ser^{73})	9164s	Cell Signaling Technology, Inc.	1:1,000
Anti-c-Jun	9165s	Cell Signaling Technology, Inc.	1:5,000
Anti-p-c-Fos (Ser^{32})	5348s	Cell Signaling Technology, Inc.	1:1,000
Anti-c-Fos	2250s	Cell Signaling Technology, Inc.	1:5,000
Anti-Smad7	365846s	Cell Signaling Technology, Inc.	1:1,000
Anti-Smad2	3108s	Cell Signaling Technology, Inc.	1:1,000
Anti-p-Smad3 ($Ser^{423/425}$)	9520s	Cell Signaling Technology, Inc.	1:1,000
Anti-Smad3	9250s	Cell Signaling Technology, Inc.	1:1,000
Anti-p-Smad2 ($Ser^{465/467}$)	12570-1-ap	Proteintech Group, Inc.	1:1,000
Anti-TGFβ-1	21898-1-ap	Proteintech Group, Inc.	1:5,000
Anti-Nrf2.	PA5-27882	Thermo Fisher Scientific, Inc.	1:1,000
Anti-Ki67	MA5-14520	Thermo Fisher Scientific, Inc.	1:500
Anti-procollagen type I	ABT-257	Merck	1:1,000
Anti-elastin	58756s	Cell Signaling Technology, Inc.	1:250

iNOS, intracellular nitric oxide synthase; MMP1, matrix metalloproteinase 1; Nrf2, nuclear factor erythroid 2-related factor 2; RAD51, radiation sensitive 51.

exposed to UVB irradiation using a BIO-SPECTRA (Vilber Lourmat Sta), three times a week for 8 weeks. Initially, the dose was set at 100 mJ/cm^2 for 2 weeks, and this was then increased to 150 mJ/cm^2 for 4 weeks. In addition, the mice were irradiated with UVB at 150 or 200 mJ/cm^2 for 2 weeks. Immediately after UVB irradiation, 100 μl BJ-5ta Exo were injected subcutaneously into the backs of the mice, three times a week. The normal mice were subcutaneously injected with saline three times a week. The wrinkles on the backs of the mice were photographed using a DSLR camera (Canon EOS 700D) and PRIMOS CR (SnTLab).

Anesthesia/euthanasia. The mice were euthanized by CO_2 asphyxiation. The mice were placed in a new cage, and immediately euthanized by the displacement of air with 100% CO_2 (30% chamber volume/min), within 5 min and decapitated for tissue collection (29,30).

Morphological analysis, histological observation and immunohistochemistry (IHC). Morphological changes in the dorsal skin were observed using a DSLR camera (Canon EOS 700D) and PRIMOS CR (SnT Lab Co., Ltd.). at 12 weeks. Mouse skin roughness (RA) was analyzed using PRIMOS

CR software version 5.8E (SnT Lab Co., Ltd.). Skin biopsies were fixed in 10% formalin for 24 h. Paraffin-embedded 3-μm-thick sections were cut, mounted on POLYSINE® Slides (Thermo Fisher Scientific, Inc.), dewaxed in xylene, and then dehydrated in an ethanol series. Hematoxylin and eosin (H&E) staining was performed to examine the histological features and skin thickness. Masson's trichome (MT) staining and Verhoeff-van Gieson (VVG) staining were performed to evaluate collagen and elastin fibers, respectively. H&E staining was performed as follows: Hematoxylin solution was applied for 5 min, followed by eosin solution (Muto Pure Chemical Co., Ltd.) for 2 min, both at RT. Additionally, Masson's trichrome staining was conducted using the following steps: The mordant solution for 25 min, 0.75% orange G solution (Muto Pure Chemical Co., Ltd.) for 1 min, Masson's B stain solution for 25 min, 2.5% phosphotungstic acid solution for 20 min, and aniline blue (Muto Pure Chemical Co., Ltd.) for 8 min, all at RT. For VVG staining, the procedure included an initial incubation in Verhoeff's solution for 1 h, followed by washing with tap water. Subsequently, samples were exposed to 2% FeCl3 (MilliporeSigma) for 5 min, followed by treatment with 5% sodium thiosulfate (MilliporeSigma). For counterstaining, slides were stained with VVG's solution for 5 min. The samples subsequently underwent dehydration using 95% alcohol, followed by two changes of 100% alcohol. For IHC, the sliced sections were subjected to antigen retrieval with Tris-EDTA at 4˚C for 15 min, incubated with BLOXALL blocking Solution (Vector Laboratories, Inc.) at RT for 30 min, and then incubated overnight at 4˚C with the primary antibodies listed in Table II, including procollagen type I, collagen type I, MMP-1, elastin and filaggrin antibodies. The slides were then incubated with HRP using the ImmPRESS® Excel Amplified Polymer Staining kit (Vector Laboratories, Inc.). The staining was developed using the 3,3'-diaminobenzidine (DAB) peroxidase substrate kit (Vector Laboratories, Inc.). To identify nuclei, the slides were counterstained with hematoxylin at RT for <1 min. The stained slides were photographed using a slide scanner (Pannoramic MIDI; 3DHISTECH Ltd.), observed using Case Viewer software (V 2.7; 3DHISTECH Ltd.), and analyzed using ImageJ software (V1.8.0; National Institutes of Health).

Assessment of skin hydration. The hydration of the dorsal skin was assessed using a Corneometer® CM 825 (Courage + Khazaka Electronic GmbH). The amount of transepidermal water loss (TEWL) was measured using a Tewameter® TM 300 (Courage + Khazaka Electronic GmbH) after 8 weeks.

Reconstructed human skin model analysis. The reconstructed human skin model Neoderm®-ED was purchased from Tego Science, Inc. Neoderm®-ED was removed from medium-containing agar and transferred onto 12-well plates for equilibration at 37˚C (5% CO_2) for 1 day. Under treatment with BJ-5ta Exo, Neoderm®-ED was irradiated with UVB (128 mJ/cm^2), and the tissue samples were incubated at 37˚C with 5% CO_2 for 48 h.

ELISA of the reconstructed human skin model. The quantitative measurement of procollagen-type I and MMP-1 production from reconstructed human skin (Neoderm®-ED) in the supernatant was conducted using a procollagen type I ELISA kit (cat. no. MK101, Takara Bio, Inc.) and a Human MMP-1 (Sandwich ELISA) ELISA kit (cat. no. ab215083, Abcam), following the manufacturer's instructions.

Statistical analysis. Data are presented as the mean ducted using a procollagen type I ELISA kit independent experiments. Data analyses were performed using unpaired one-way analysis of variance (ANOVA) followed by the Bonferroni post hoc test. Statistical analysis was performed using GraphPad Prism 7.0 software (GraphPad Software Inc.). All experiments were repeated at least three times.

Results

Treatment with BJ-5ta Exo attenuates the UVB-irradiation-induced inhibition of cell viability. BJ-5ta-Exo exhibited a spherical morphology (Fig. 1A). The number and size of the total particles were quantified using NTA as follows: The mean size of the exosomes was 215.4±116.1 nm and the number was $2.33x10^{10}$±$2.22x10^9$/ml (Fig. 1B). The two positive markers for the exosomes (ALIX and CD63) were abundant in the BJ-5ta-Exo, while the negative protein marker, calnexin, was absent in the BJ-5ta Exo (Fig. 1C). The BJ-5ta cells were treated with BJ-5ta Exo (10^3 to 10^7 particles/ml) for 24 h, and cell viability was then measured using WST-8 assay. BJ-5ta Exo at doses of up to 10^6 particles/ml was not toxic to the BJ-5ta cells (Fig. 1D). UVB irradiation inhibited cell viability by 36 and 46% at doses of 30-40 mJ/cm^2, respectively (Fig. 1E). However, BJ-5ta Exo (10^4 particles/ml) prevented the inhibition of cell viability induced by UVB (Fig. 1F). In addition, UVB significantly decreased the percentage of cells expressing Ki67. Conversely, BJ-5ta Exo reversed this trend (Fig. 1G).

BJ-5ta-Exo treatment reduces UV-induced oxidative stress. UVB-mediated ROS generation can trigger genes related to skin photoaging and lead to oxidative stress. UVB significantly increased intracellular ROS levels compared to the control group, while BJ-5ta Exo attenuated ROS generation induced by UVB (Fig. 2A and B). UVB irradiation induced a decrease in the mRNA levels of antioxidant enzymes (*SOD-1, SOD-2, CAT* and *GPX*); however, BJ-5ta Exo prevented the downregulation of these genes (Fig. 2C). Furthermore, UVB irradiation resulted in the downregulation of NF-E2-related factor 2 (Nrf2), which is responsible for inducing the transcription of antioxidant and cytoprotective genes. However, BJ-5ta Exo attenuated this decrease in Nrf2 expression (Fig. 2D). In addition, it was confirmed that BJ-5ta Exo inhibited the UVB-mediated decrease of Nrf2 in the nucleus (Fig. 2E). These results thus suggested that BJ-5ta Exo suppressed UVB-induced oxidative stress by increasing the expression levels of Nrf2.

BJ-5ta Exo reduce UVB-induced DNA damage, p53/p21 pathway activation and senescence. UVB exposure caused an increase in γH2AX expression, while BJ-5ta Exo suppressed this increase (Fig. 3A). Using ICC staining (Fig. 3B), it was found that BJ-5ta Exo inhibited the UVB-induced γH2AX foci and nuclear accumulation.

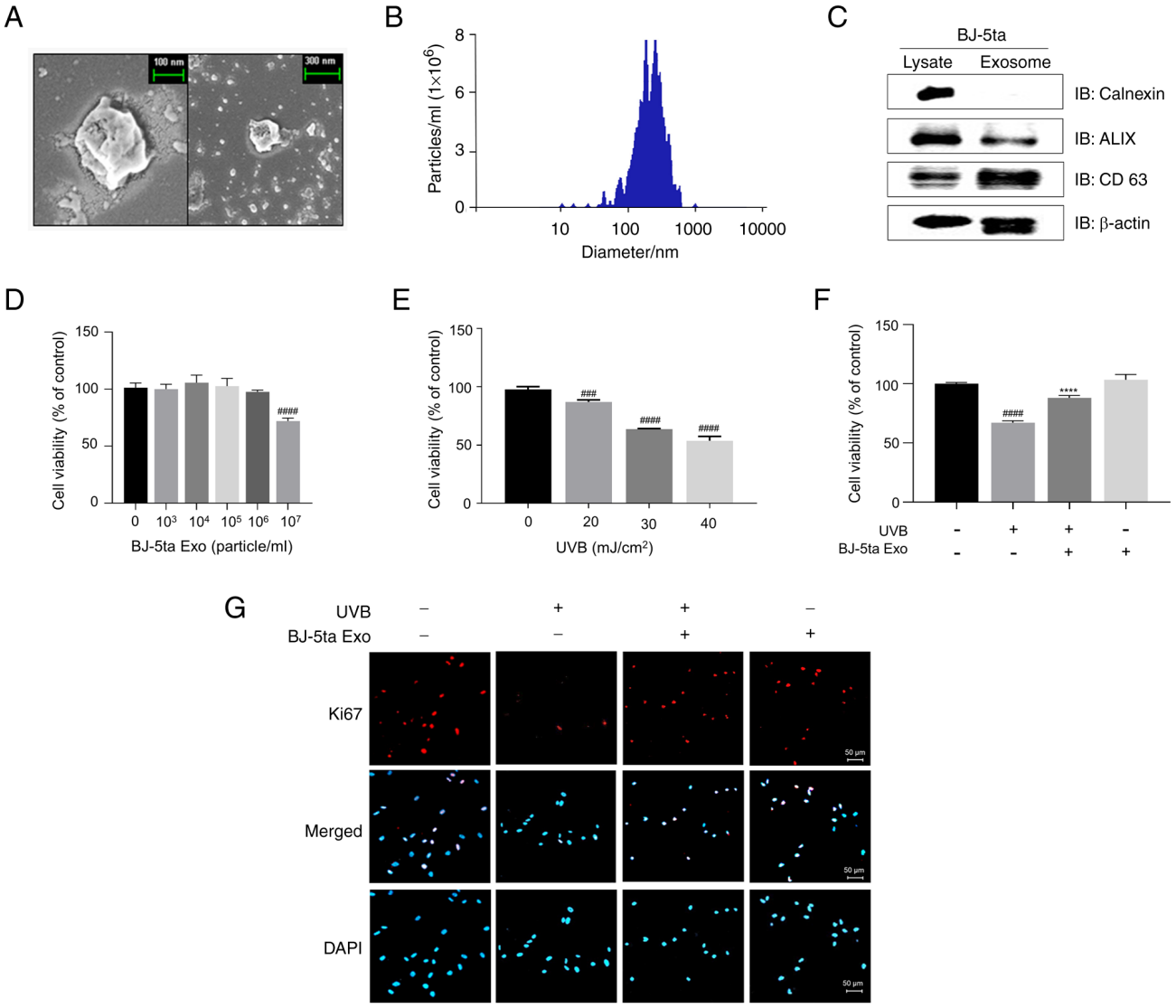

Figure 1. Characterization of BJ-5ta Exo and its effects on cell viability. (A) Representative image of BJ-5ta Exo obtained using a field emission scanning electron microscope (FE-SEM). Scale bar, 100 nm (left panel) and 300 nm (right panel). (B) Representative histogram illustrating the particle concentration and size distribution of BJ-5ta Exo measured by nanoparticle tracking analysis. (C) Expression of CD63, ALIX and calnexin in BJ-5ta-Exo as determined using western blot analysis. (D) BJ-5ta cells were treated with BJ-5ta-Exo (10^3-10^6 particles/ml) for 24 h, followed by cell viability analysis using the WST-8 cell viability assay. (E) Cell viability examined in UVB-irradiated cells at various concentrations. (F) The protective effect of BJ-5ta Exo (10^4 particles/ml) on UVB-irradiated BJ-5ta cells (30 mJ/cm^2) as assessed using the WST-8 cell viability assay. (G) Immunocytochemistry was performed using Ki-67 (in red) and DAPI (in blue) on BJ-5ta cells pre-treated with BJ-5ta Exo (10^4 particles/ml) for 6 h, followed by irradiation with UVB (30 mJ/cm^2) and 24 h of culture. Scale bar, 50 μm. ****P<0.0001, compared with UVB-irradiated cells; $^{###}$P<0.001 and $^{####}$P<0.0001s compared with normal cells. BJ-5ta Exo, exosomes derived from BJ-5ta cells; UVB, ultraviolet B.

BJ-5ta Exo also prevented the UVB-induced upregulation of RAD51 and cleaved PARP-1 (Fig. 3C). In addition, the apoptotic cells were analyzed using Annexin V and PI solution followed by flow cytometric analysis. UVB irradiation increased total apoptosis by 20.9% compared to the control group. However, BJ-5ta Exo significantly reduced apoptosis, resulting in an 11.39% inhibition compared to the UVB-alone group (Fig. 3D). Cell cycle analysis also revealed that UVB irradiation decreased the cell populations in the G0/G1 phase (from 82.73±1.38 to 62.30±5.31%). However, BJ-5ta Exo partially prevented the G2-phase cell cycle alteration compared with the UVB group (from 16.90±4.20 to 9.32±0.41) (Fig. 3E). Subsequently, it was confirmed that BJ-5ta Exo efficiently reversed the UVB-mediated increase in p53 and p21 expression (Fig. 3F). The number of cells expressing SA-β-Gal and the expression levels of p16 were also significantly increased after UVB irradiation compared to the control cells; however, these effects were attenuated by BJ-5ta Exo (Fig. 3G and H).

BJ-5ta Exo alleviate UVB-induced inflammation. UVB increased COX-2 and iNOS expression (4.0-fold and 1.4-fold, respectively, compared to the control group), while BJ-5ta Exo significantly reduced the COX-2 and iNOS levels by 0.3-fold compared to the UVB-only group (Fig. 4A). The levels of p-NF-kB (Ser^{536}) were found to be elevated by UVB, although this effect was reversed by BJ-5ta Exo (Fig. 4B). Furthermore, ICC staining confirmed that BJ-5ta Exo significantly inhibited the UVB-induced translocation of NF-κB to the nucleus (Fig. 4C).

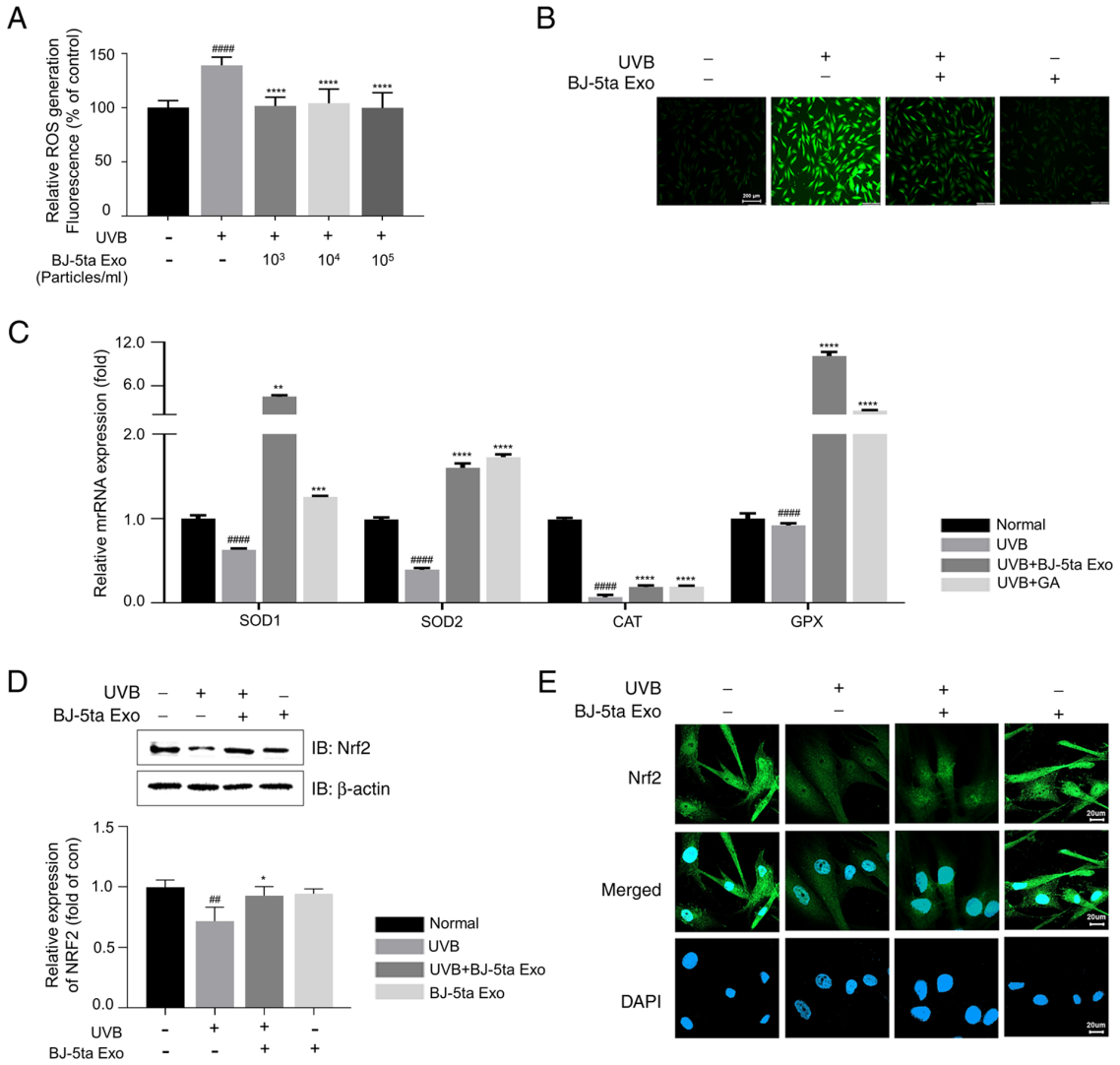

Figure 2. Effects of BJ-5ta Exo on intercellular ROS levels. (A) UVB-induced intracellular ROS generation was attenuated by BJ-5ta Exo (10^3,10^4 and 10^5 particles/ml) in BJ-5ta cells. (B) Representative intracellular ROS images of cells pre-treated with BJ-5ta Exo (10^4 particles/ml) for 6 h, followed by UVB (30 mJ/cm^2) irradiation. Scale bar, 200 μm. (C) The mRNA expression levels of Nrf2 downstream antioxidant enzymes (SOD-1 or 2, CAT and GPX). (D) Total Nrf2 protein levels. (E) Nrf2 localization was determined using immunocytochemistry with an anti-Nrf2 antibody (green fluorescence) and DAPI staining (blue fluorescence). Scale bar, 20 μm. BJ-5ta cells were pre-treated with BJ-5ta Exo (10^4 particles/ml) for 6 h, followed by exposure to UVB (30 mJ/cm^2). Following 3 h of incubation (C-E), the cells were analyzed using RT-qPCR, western blot analysis, or immunocytochemistry. *P<0.05, **P<0.01, ***P<0.001 and ****P<0.0001, compared with UVB-irradiated cells; $^{\#\#}$P<0.01, $^{\#\#\#\#}$P<0.0001, compared with normal cells. BJ-5ta Exo, exosomes derived from BJ-5ta cells; UVB, ultraviolet B; ROS, reactive oxygen species; SOD, superoxide dismutase; CAT, catalase; GPX, glutathione peroxidase; Nrf2, nuclear factor erythroid 2-related factor 2.

BJ-5ta Exo reverse the UVB-induced increase in MMP-1 and the decrease in collagen type I expression through the MAPK/AP-1/TGF-β1/Smad signaling pathway. BJ-5ta Exo suppressed the UVB-induced decrease in collagen type I levels, while increasing MMP-1 expression (Fig. 5A). The TGF-β1 signaling pathway plays a key role in the regulation of ECM biosynthesis, including procollagen (31). As shown in Fig. 5B, UVB significantly decreased TGF-β1 expression, as well as the phosphorylation levels of Smad2 (Ser$^{465/467}$) and Smad3 (Ser$^{423/425}$), which were reduced by 0.2-fold, while the level of Smad7 increased by 1.3-fold compared to the control group. However, BJ-5ta Exo inhibited the UVB-induced suppression of the TGF-β1/Smad pathway. The UVB-induced production of MMPs can be mediated by protein kinase cascades, such as MAPK and AP-1 (32). BJ-5ta Exo prevented the UVB-mediated increase in the levels of p-p38 (Thr^{180}/Tyr^{182}), p-JNK (Thr^{183}/Tyr^{185}) and p-ERK(Thr^{202}/Tyr^{204}) (Fig. 5C). In addition, BJ-5ta Exo suppressed the UVB-induced phosphorylation of AP-1 subunits (c-Fos on Ser^{32} and c-Jun on Ser^{73}) (Fig. 5D).

BJ-5ta-Exo reduce UVB-induced wrinkle formation by suppressing collagen degradation and decreasing MMP-1 expression. To examine whether BJ-5ta Exo reduce wrinkle formation caused by UVB irradiation in SKH-1 hairless mice, BJ-5ta Exo were subcutaneously injected into the dorsal skin of each group of mice for 8 weeks following irradiation with UVB (Fig. S2A). Ultimately, there was no significant difference in the body weights of the mice treated with various concentrations of BJ-5ta Exo alongside UVB exposure, indicating the safety of BJ-5ta Exo for the mice (Fig. S2B). A visual assessment indicated that the administration of BJ-5ta Exo reduced the

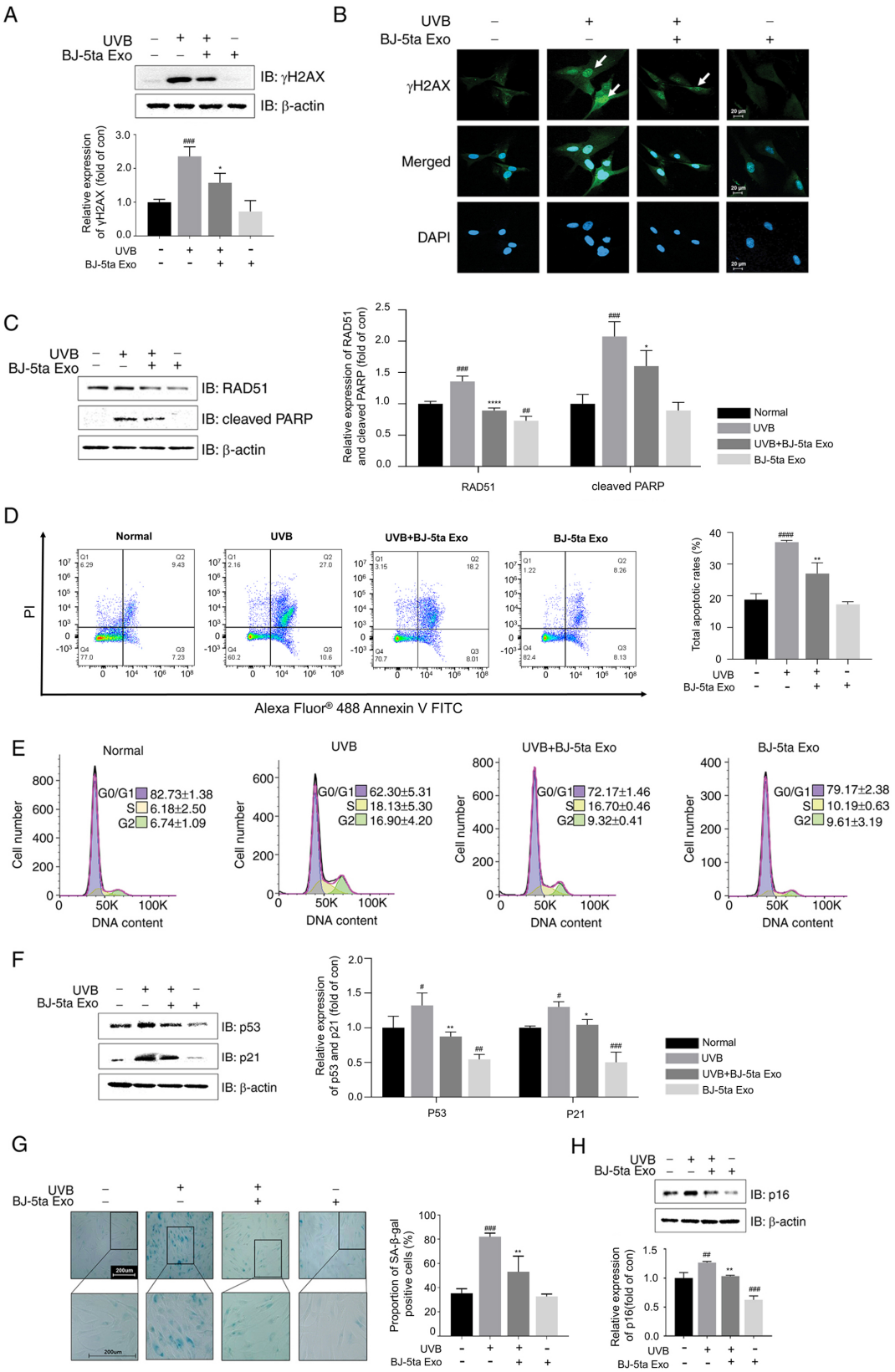

Figure 3. Effects of BJ-5ta Exo on UVB-induced DNA damage, the p53/p21 pathway and senescence in BJ-5ta cells. (A) Cell lysates were analyzed using western blot analysis with antibodies against γH2AX. (B) The expression of γH2AX was determined using immunocytochemistry with an anti-γH2AX antibody (green fluorescence) and DAPI (blue fluorescence). Scale bar, 20 μm. Protein levels of (C) RAD51 and cleaved PARP were analyzed using western blot analysis. (D) Apoptosis and (E) cell cycle distribution was analyzed using flow cytometry. (F) The levels of p53, and its downstream effector p21, were assessed using western blot analysis. (G) SA-β-Gal-positive cells were observed in BJ-5ta cells pre-treated with and without BJ-5ta Exo (10^4 particles/ml) and exposed to UVB (30 mJ/cm^2). Scale bar, 200 μm. (H) The protein levels of p16, a marker of cellular senescence, were determined using western blot analysis. Cells were pre-treated with and without BJ-5ta Exo (10^4 particles/ml) for 6 h and then exposed to UVB radiation (30 mJ/cm^2). Following 24 h of incubation, the cells were analyzed using western blot analysis or immunocytochemistry. In western blot analysis, the protein levels were quantified and presented relative to the β-actin levels. The results are expressed as the mean ± standard deviation. *P<0.05, **P<0.01 and ****P<0.0001, compared with UVB-irradiated cells; $^{\#}$P<0.05, $^{\#\#}$P<0.01, $^{\#\#\#}$P<0.001 and $^{\#\#\#\#}$P<0.0001, compared with normal cells. BJ-5ta Exo, exosomes derived from BJ-5ta cells; UVB, ultraviolet B; SA-β-Gal, senescence-associated β-galactosidase.

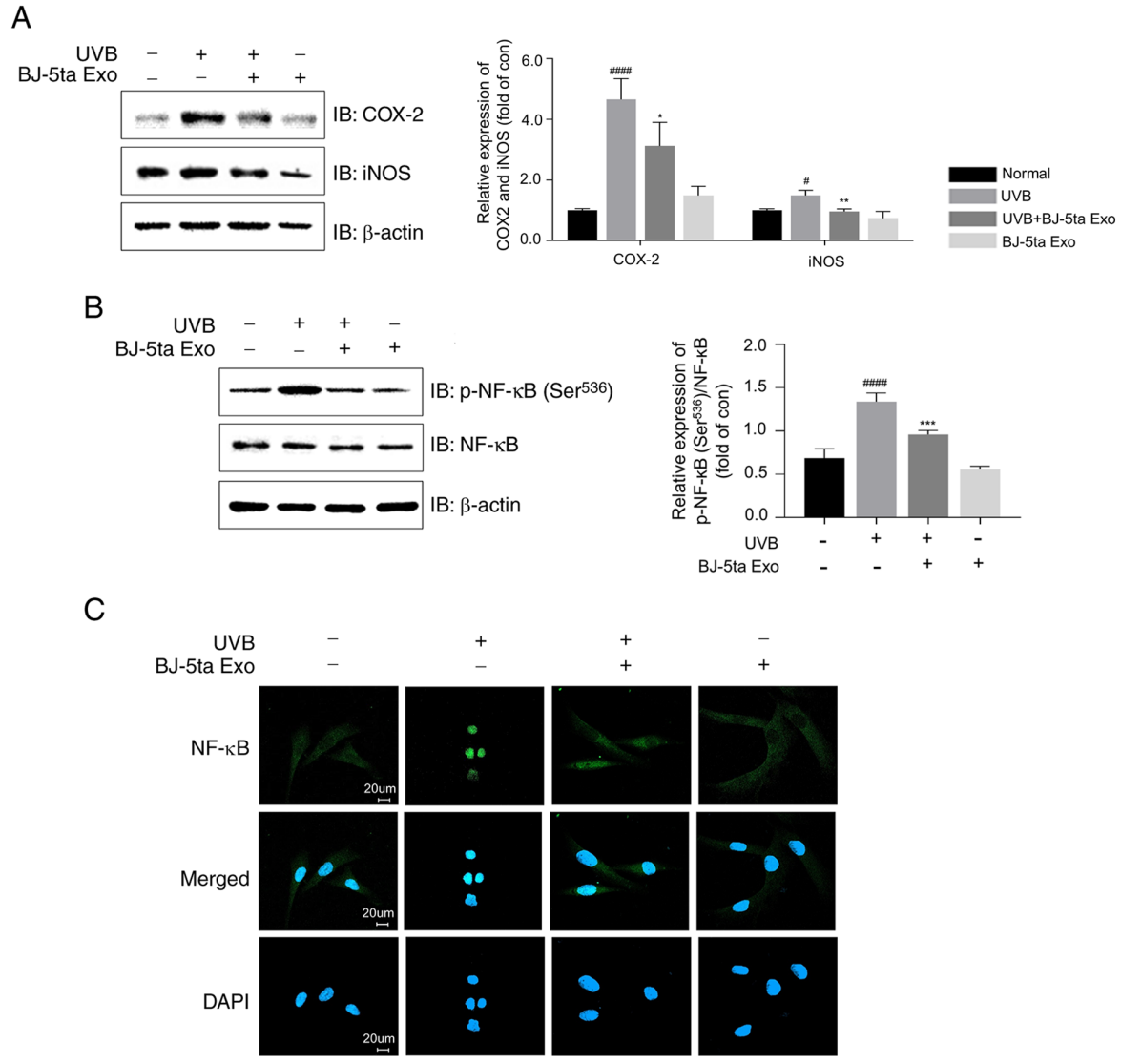

Figure 4. Inhibition of UVB-induced expression of p-NF-κB, iNOS and COX-2 by BJ-5ta Exo. BJ-5ta cells were treated with and without BJ-5ta-Exo for 6 h and then irradiated with UVB (30 mJ/cm^2). After 24 h, cell lysates were examined using western blot analysis for the protein levels of (A) COX-2 and iNOS, and (B) p-NF-κB (Ser^{536}). (C) NF-κB localization was determined using immunocytochemistry with an anti-NF-κB antibody (green fluorescence) and DAPI (blue fluorescence). The levels of the phosphorylated proteins were normalized to β-actin or total NF-κB proteins. The results are expressed as the mean ± standard error. P<0.05, **P<0.01, ***P<0.001 compared with UVB-irradiated cells; $^{\#\#}$P<0.01, $^{\#\#\#\#}$P<0.0001 compared with normal cells. BJ-5ta Exo, exosomes derived from BJ-5ta cells; UVB, ultraviolet B; iNOS, inducible nitric oxide synthase; COX-2, cyclooxynase 2.

UVB-induced wrinkle formation on the back skins of the mice compared to the saline-treated UVB-irradiated mice (Fig. 6A). To quantitatively measure the roughness, relevant parameters in the images were analyzed using PRIMOS CR software version 5.8E, an optical three-dimensional skin measurement system. The roughness values in the UVB-saline group were significantly higher (1.4-fold) compared with those in the control group. By contrast, the mice treated with BJ-5ta Exo at concentrations of 1x10^6 particles/ml and 1x10^8 particles/ml exhibited a reduction in total wrinkle area of 0.3- and 0.4-fold, respectively, compared to the saline-treated group (Fig. 6E). BJ-5ta Exo also restored skin hydration and inhibited moisture evaporation compared to the UVB-saline group (Fig. 6F and G). As shown in Fig. 6H and I-K, the saline-treated UVB-irradiated mice had a thicker epidermal surface and a marked decrease in collagen (blue) and elastin (black) fibers in the dermis compared to the control mice, while the treated mice exhibited a significant increase in the abundance and density of collagen and elastin fibers in the dermis, and a significant decrease in the thickness of the epidermal layer. In addition, using IHC staining, it was observed that the expression levels of procollagen type I, collagen type I and elastin were restored by 1.4, 1.3, and 1.3-fold, respectively, in the BJ-5ta Exo 10^6-treated group, and by 1.5, 1.3, and 1.3-fold, respectively, in the BJ-5ta Exo 10^8-treated group, compared to the UVB-saline group. By contrast, MMP-1 expression decreased by 0.3-fold in the BJ-5ta Exo 10^6-treated group and 0.4-fold in the BJ-5ta Exo 10^8-treated group (Fig. 6L and M). These results suggest that BJ-5ta Exo can ameliorate skin photodamage by increasing ECM components.

BJ-5ta Exo inhibit UVB-induced MMP-1 expression and collagen reduction in a reconstructed human skin model. To further investigate the effects of BJ-5ta Exo on UVB-induced photodamage in human skin, the Neoderm-ED reconstructed

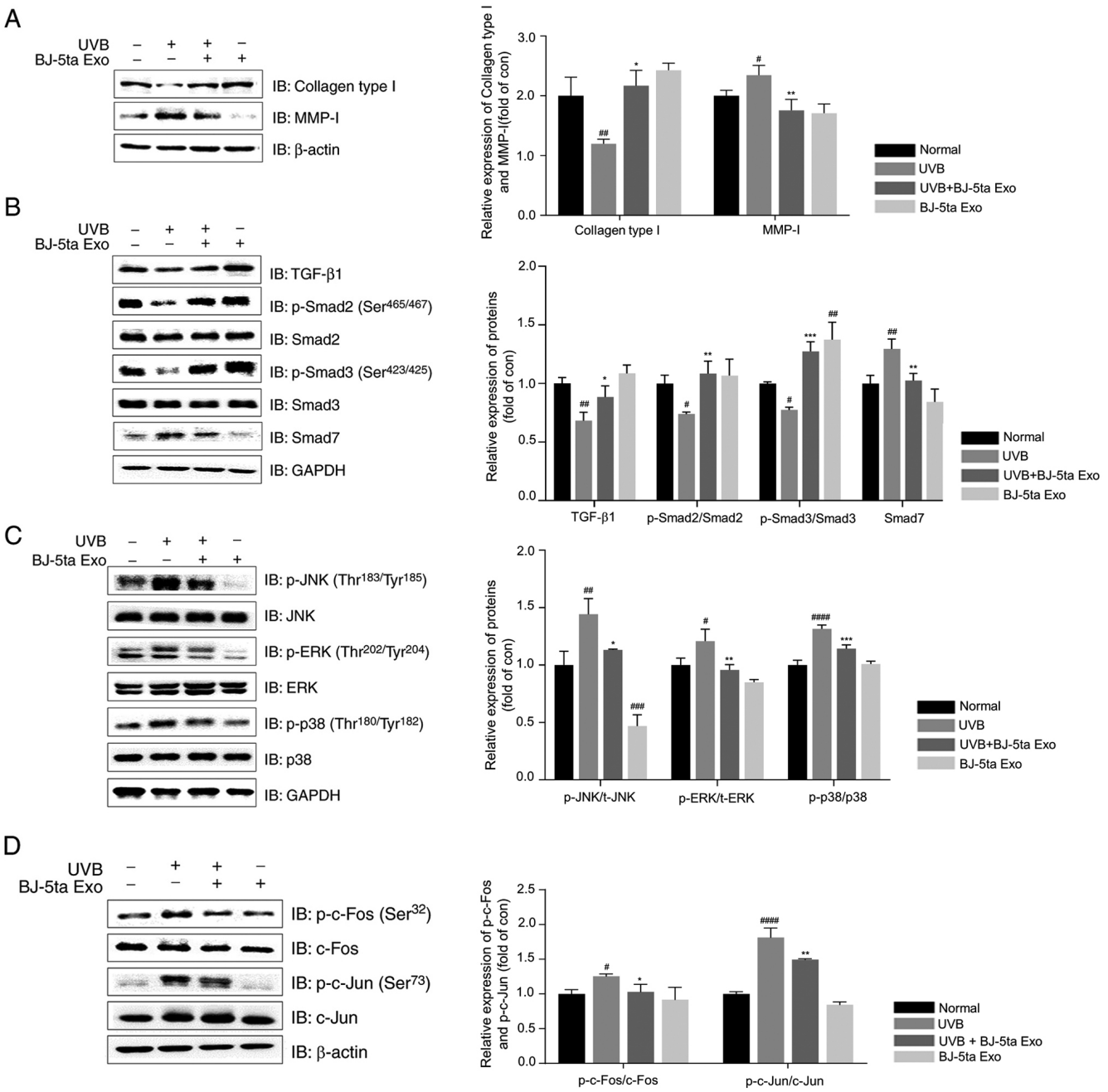

Figure 5. Effects of BJ-5ta Exo on the levels of collagen type I, MMP-I, TGF-β1/Smads and MAPK/AP-1 phosphorylation in UVB-irradiated BJ-5ta fibroblasts. Protein levels of (A) collagen type I and MMP-1; (B) TGF-β1, p-Smad2 ($Ser^{465/467}$), p-Smad3 ($Ser^{423/425}$) and Smad7; (C) p-JNK (Thr^{183}/Tyr^{185}), p-ERK (Thr^{202}/Tyr^{204}), and p-p38 (Thr^{180}/Tyr^{182}); (D) p-c-Fos (Ser^{32}) and p-c-Jun (Ser^{73}) were examined using western blot analysis. Cells were pre-treated with and without BJ-5ta Exo (10^4 particles/ml) for 6 h and then exposed to UVB radiation (30 mJ/cm^2). Following (A) 24 h or (B-D) 30 min of incubation, the cells were examined using western blot analysis. The levels of the phosphorylated proteins were normalized to β-actin or total proteins. The results are expressed as the mean ± standard error. *P<0.05, **P<0.01, ***P<0.001 compared with UVB-irradiated cells; $^{\#}$P<0.05, $^{\#\#}$P<0.01, $^{\#\#\#}$P<0.001 and $^{\#\#\#\#}$P<0.0001 compared with normal cells. BJ-5ta Exo, exosomes derived from BJ-5ta cells; UVB, ultraviolet B; MMP, matrix metalloproteinase.

human skin model was employed. The thickness of the epidermis increased as a result of UVB exposure. However, BJ-5ta Exo effectively reduced the increased epidermal thickness caused by UVB (Fig. 7A and E). UVB radiation causes an abnormal reduction in procollagen type I and elastin, as well as the production of MMP-1. Using IHC staining for collagen type I, elastin and MMP-1, it was confirmed that BJ-5ta Exo inhibited the UVB-induced downregulation of collagen type I and elastin, while also suppressing the UVB-induced increase in MMP-1 (Fig. 7B-D). In addition, ELISA assay used to quantify procollagen type I and MMP-1. Compared to the UVB-alone group, the groups treated with BJ-5ta Exo at concentrations of 10^6 and 10^8 particles/ml exhibited an elevated expression of procollagen type I, with an increased rate of 34.53 and 35.30%, respectively. Additionally, they exhibited a decrease in MMP-1 levels by 6.85 and 20.14%, respectively. (Fig. 7F and G). These observations indicated that BJ-5ta Exo effectively restored the tissue damage induced by UVB in the layers of the reconstructed human skin model.

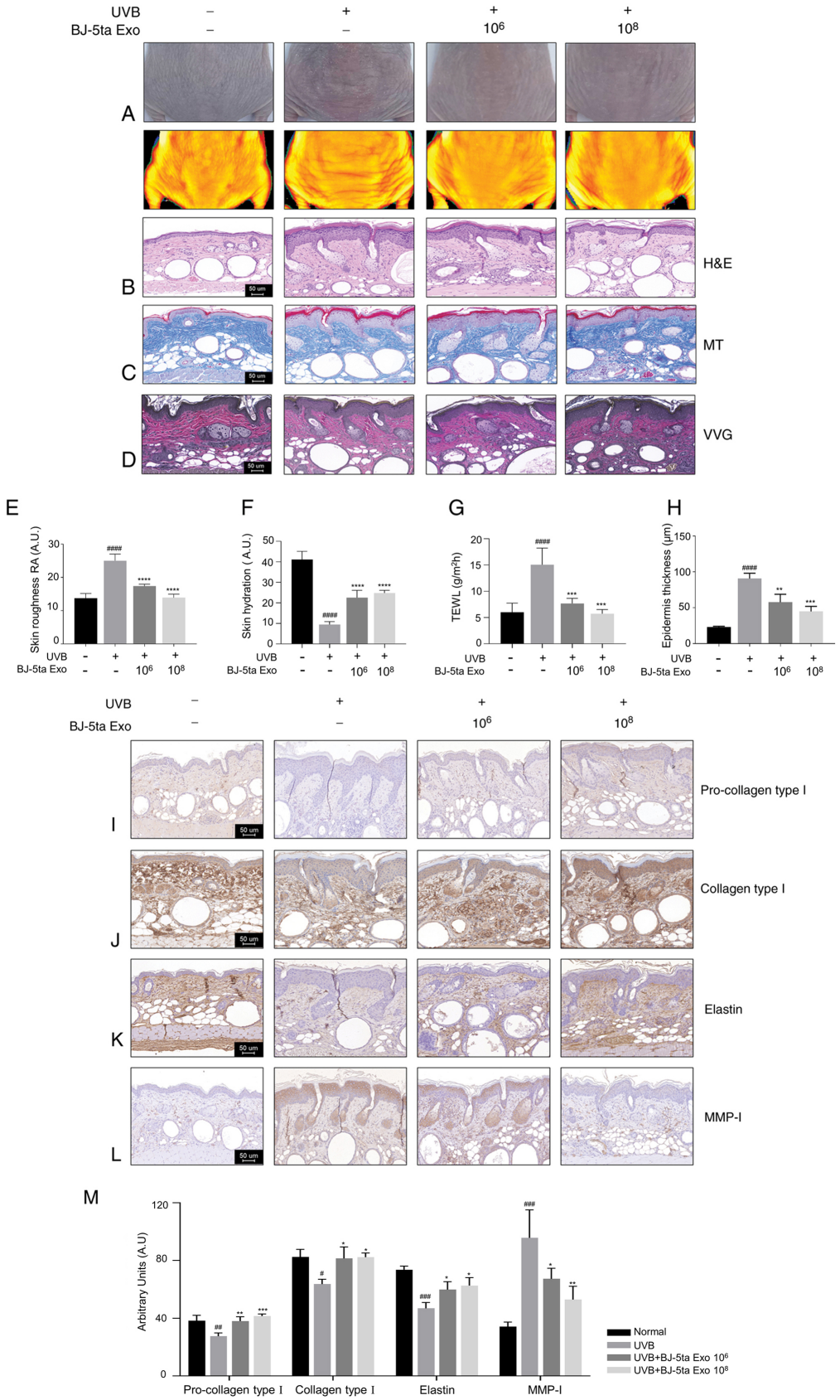

Figure 6. Subcutaneous injection of BJ-5ta Exo attenuates UVB-induced wrinkle formation in skin of mice. (A) To evaluate the changes in dorsal wrinkle formation, images were obtained using a DSLR and PRIMOS CR. (B) H&E staining. (C) MT staining. (D) VVG staining. (E) The quantification of wrinkles (roughness) revealed that the depth of the wrinkles was reduced by BJ-5ta Exo. RA, average roughness. (F) Skin hydration was evaluated using a Corneometer. (G) TEWL was evaluated using a Tewameter TM300. (H) Epidermal thickness was quantified using ImageJ software. (I) Procollagen type I, (J) collagen type I, (K) elastin, and (L) MMP-1 were analyzed using immunohistochemistry. Scale bar, 50 μm. (M) Immunohistochemistry arbitrary units (a.u.) of procollagen type I, collagen type I, MMP-1 and elastin in SKH-1 mice. The results are expressed as the mean ± standard error. *P<0.05, **P<0.01, ***P<0.001 and ****P<0.0001, compared with UVB irradiation; $^{\#}$P<0.05, $^{\#\#}$P<0.01, $^{\#\#\#}$P<0.001 and $^{\#\#\#\#}$P<0.0001, compared with the control. BJ-5ta Exo, exosomes derived from BJ-5ta cells; UVB, ultraviolet B; H&E, hematoxylin and eosin; MT, Masson's trichome; VVG, Verhoeff-van Gieson; TEWL, transepidermal water loss.

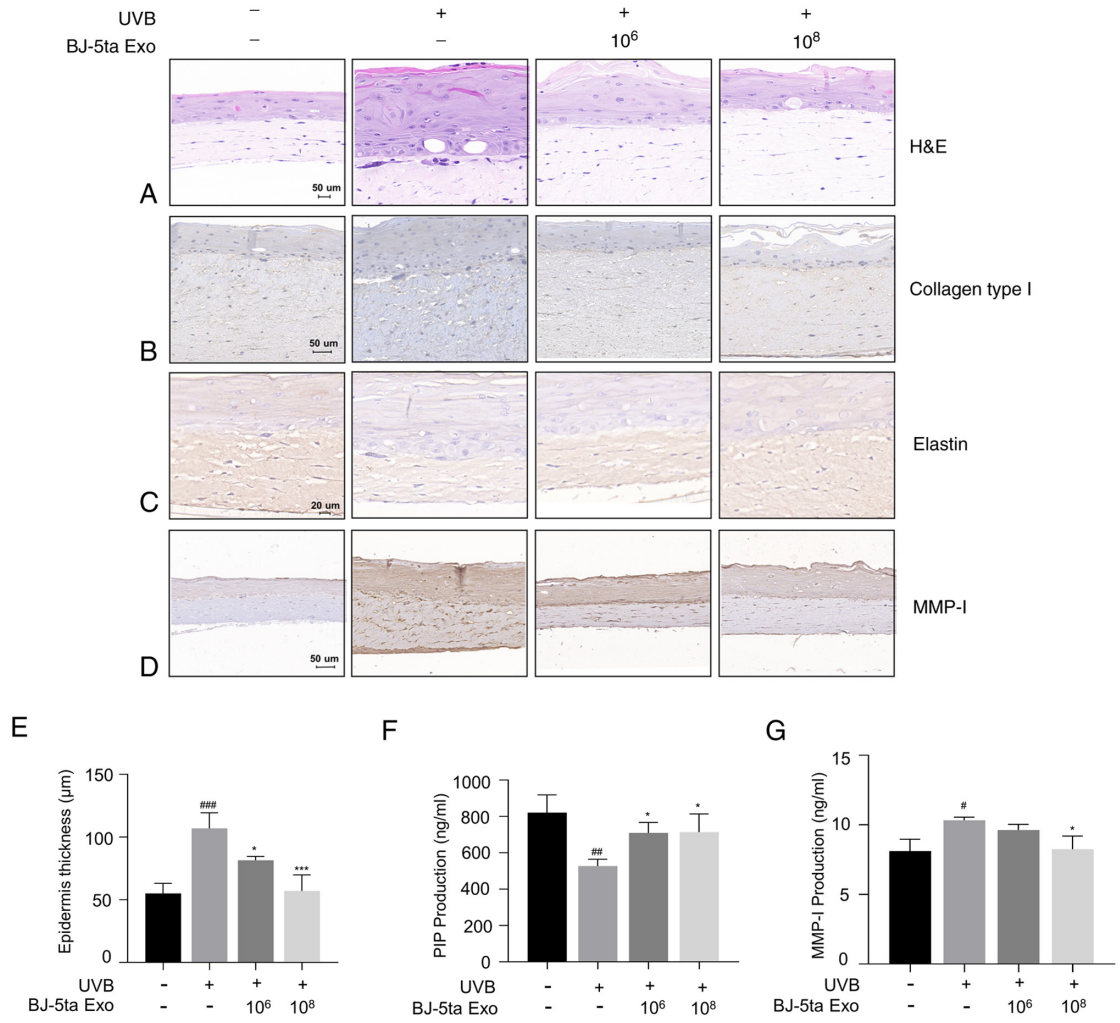

Figure 7. Protective effects of BJ-5ta Exo on UVB-induced photoaging was evaluated using a reconstructed human skin model, Neoderm®-ED. The impact of BJ-5ta Exo on UVB-induced skin tissue damage was assessed. Following UVB irradiation, the skin tissues were subjected to staining with (A) H&E, (B) collagen type I, (C) elastin, and (D) MMP-1. (E) Epidermal thickness was quantified using ImageJ software. (F) PIP and (G) MMP-1 expression levels were analyzed using ELISA. The reconstructed human skin model was exposed to UVB (128 mJ/cm^2), and the supernatants were collected after 48 h. BJ-5ta Exo, exosomes derived from BJ-5ta cells; UVB, ultraviolet B; H&E, hematoxylin and eosin; MMP, matrix metalloproteinase; PIP, procollagen type I C peptide. *P<0.05 and ***P<0.001, compared with UVB irradiation; $^{\#}$P<0.05, $^{\#\#}$P<0.01 and $^{\#\#\#}$P<0.001, compared with the control.

Working model of BJ-5ta exosome with anti-photoaging effects. BJ-5ta Exo treatment contributes to the removal of oxidative stress by inhibiting ROS generation and preventing the decrease in the expression levels of SOD1 and SOD2, GPX and catalase. It also provides protection against UVB radiation by activating the DNA repair system through the regulation of both γH2AX and RAD51. BJ-5ta Exo prevent UVB-induced collagen degradation by activating the TGF-β1/Smads pathway and inhibiting the MAPK/AP-1 pathway. Furthermore, BJ-5ta Exo suppress UVB-induced cellular senescence by inhibiting the expression of SA-β-gal and p16. In a UVB-induced photoaging model, it was confirmed that BJ-5ta-Exo treatment decreased the level of TEWL, wrinkle formation and MMP-1 expression. On the other hand, BJ-5ta Exo increased the levels of collagen type-I and elastin in the dorsal skin (Fig. 8).

Discussion

Recently, there has been extensive research on the effects of exosomes on various skin defects. Exosomes have several key benefits, including high stability, non-immune rejection and the ability to directly stimulate target cells (20,33). Exosomes derived from ADSCs or mesenchymal stem cells play crucial roles in aging, atopic dermatitis and wound healing (34,35). Moreover, recent studies have found that exosomes derived from autologous hDFs can more effectively promote cutaneous wound healing (36,37), indicating that exosomes from hDFs may be potential materials for protecting and repairing skin damage.

In addition to the effects mentioned above, there have been reports on the photoprotective effects of exosomes against UVB damage. Gao *et al* (38) investigated the role of ADSCs-Exo in hDFs exposed to UVB radiation. They found that ADSCs-Exo treatment attenuated UVB-induced photoaging in hDFs (38). In addition, Ellistasari *et al* (39) reported that exosomes derived from human umbilical vein endothelial cells (HUVEC-Exo) ameliorated UVB-induced photoaging in skin fibroblasts. These findings indicate that exosomes are effective in preventing UVB-mediated dermal photoaging in *in vitro* models. The present study further investigated the effects of BJ-5ta-Exo on a UVB-irradiated photoaging model using human neonatal

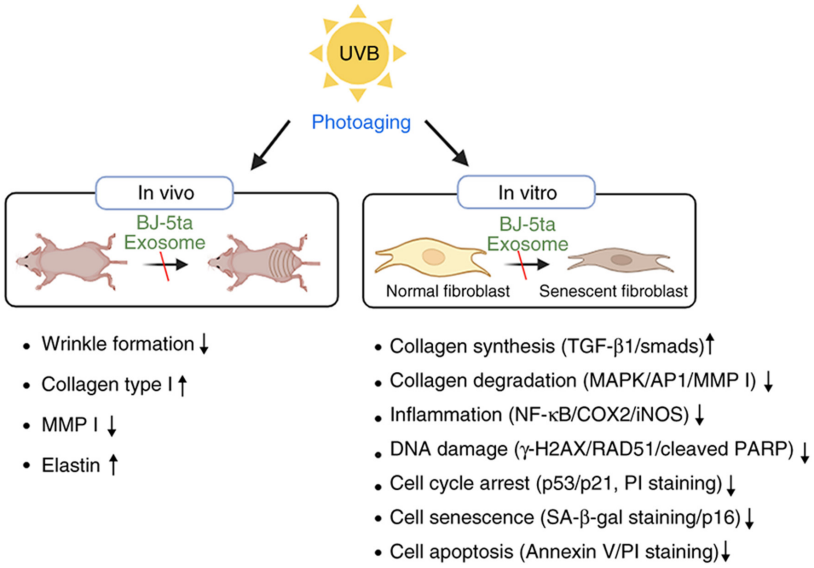

Figure 8. BJ-5ta Exo exert a protective effect against UVB-induced photoaging. BJ-5ta Exo protect against UVB-mediated winkle formation by inhibiting the MAPK/AP-1 signaling pathway and subsequent MMP-1 release and activating collagen synthesis. Furthermore, BJ-5ta Exo inhibited inflammation, apoptosis, cell cycle arrest and DNA damage caused by UVB exposure. Overall, these findings suggest that BJ-5ta Exo may be a valuable anti-photoaging agent for cosmetic products. BJ-5ta Exo, exosomes derived from BJ-5ta cells; UVB, ultraviolet B; MMP, matrix metalloproteinase.

foreskin fibroblast BJ-5ta, SKH1 hairless mice and a reconstructed human skin model, as well as its mechanism of action.

The skin barrier, mainly composed of the epidermis, serves as a physical barrier against pathogens, irritants and UV radiation. It also prevents water and solute loss, while maintaining homeostasis (40). Exposure to UVB radiation can impair the function of the epidermis barrier, leading to sunburn, skin dryness and an increased thickness of the epidermis (41). The present study found that BJ-5ta-Exo prevented the loss of skin hydration, the increase in TEWL and epidermal hyperplasia (Fig. 6F-H). Furthermore, it was confirmed that the levels of filaggrin, which plays a key role in the skin barrier (42), increased in the dorsal skin of mice treated with BJ-5ta-Exo prior to UVB radiation (Fig. S3). Collectively, these results suggest that BJ-5ta-Exo has the ability to maintain a healthy skin barrier against UVB radiation.

As shown in Fig. 2C, BJ-5ta Exo increased the expression of *CAT, SOD-1, SOD-2 and GPX*, indicating that BJ-5ta-Exo can alleviate UVB-induced oxidative stress by stimulating the expression antioxidant-related genes. The Nrf2 transcription factor is a key regulator of cellular oxidative stress (43). Under UVR exposure, Nrf2 is typically translocated from the cytoplasm to the nucleus, where it activates various target genes, including heme oxygenase-1, NAD(P)H quinone dehydrogenase 1, glutamate-cysteine ligase and glutathione synthetase, which help mitigate cellular oxidative stress (44). However, if UVR increases extremely, the balance of defense systems such as Nrf2 be disrupted (13). As shown in Fig. 2D and E, BJ-5ta Exo suppressed UVB-mediated Nrf2 downregulation, which suggests that BJ-5ta Exo attenuated UVB-induced oxidative stress by increasing Nrf2 activity.

RAD51 plays a central role in eukaryotic homologous recombination (HR), where it identifies and invades homologous DNA sequences to facilitate the accurate and timely repair of the DNA (45). The phosphorylated form of histone H2AX (γH2AX) is widely regarded as the most sensitive indicator of DSB formation (46). BJ-5ta Exo attenuated the induction of γH2AX by UVB irradiation. Mechanistically, BJ-5ta Exo functioned by downregulating RAD51, which in turn promoted the repair of damaged DNA (Fig. 3A and B).

The increased ROS production induced by UVB may result in the activation of p53 and p21, which are hallmarks of cellular senescence associated with cell cycle arrest and decreased cell proliferation (47). As shown in Fig. 3F, BJ-5ta Exo alleviated the UVB-induced increase in p53 and p21. The protein c-PARP serves as a marker for cells undergoing apoptosis (48). BJ-5ta Exo also inhibited the UVB-induced increase in cleaved PARP levels. In addition, it was confirmed that BJ-5ta-Exo reduced cell cycle arrest and apoptosis (Fig. 3D and E), indicating that BJ-5ta Exo promote DNA repair, resulting in a decrease in cellular apoptosis and prompting cell cycle arrest.

Collagen and elastin networks comprise the majority of the ECM in the skin. Collagen constitutes ~70% of the dermal layer and provides tensile stiffness and strength, whereas the biopolymer elastin, in the form of elastic fibers, provides compliance and supports stress during multiaxial deformation (49). UVB not only hinders collagen synthesis and promotes its breakdown, but also boosts the degradation of elastin in fibroblasts (50). It was observed that BJ-5ta-Exo attenuated UVB-mediated wrinkle formation (Fig. 6A and E). Consistent with these findings, BJ-5ta Exo suppressed the UVB-mediated decrease in procollagen type I, collagen type I and elastin. Additionally, BJ-5ta Exo downregulated the UVB-induced increase in MMP-1 levels (Fig. 7D and G). These results strongly support the effectiveness of BJ-5ta Exo against UVB-induced photoaging. Indeed, exosomes contain proteins, lipids and RNAs that are specific to their cell origin and could deliver cargo to both nearby and distant cells. As a result, the investigation of exosome cargo contents may provide offer opportunities for disease detection and treatment. Therefore, the authors aim to analyze protein cargo using liquid chromatography-mass spectrometry in future studies.

In conclusion, the findings of the present study indicate that BJ-5ta Exo have the potential to serve as a preventive and therapeutic option for improving photoaging-associated skin diseases.

Acknowledgements

Not applicable.

Funding

The present study was supported by the Chung-Ang University Research Scholarship Grants in 2023.

Availability of data and materials

The analyzed data sets generated during the present study are available from the corresponding author on reasonable request.

Authors' contributions

AYP was involved in the study methodology, investigation, data curation, formal analysis, and in the writing of the manuscript. JOL was involved in the writing, reviewing and editing of the manuscript, as well as in data investigation and data curation, and in funding acquisition. YNJ, YJK, SYK, and JML were involved in data investigation and data curation. KHY was involved in the conceptualization of the study, in data investigation, and in the reviewing and editing of the manuscript. BJK was involved in the conceptualization and methodology of the study, in data investigation, and in project administration. All authors have read and approved the final manuscript. JOL and NYJ confirm the authenticity of all the raw data.

Ethics approval and consent to participate

All animal experiments were conducted in accordance with the principles of laboratory animal care at the National Institutes of Health and with the approval of the Ethics Committee for Laboratory Animals at Chung-Ang University (IACUC no. A2022053).

Patient consent for publication

Not applicable.

Competing interests

The authors declare that they have no competing interests.

References

1. Kageyama H and Waditee-Sirisattha R: Antioxidative, anti-inflammatory, and anti-aging properties of mycosporine-like amino acids: Molecular and cellular mechanisms in the protection of skin-aging. Marine Drugs 17: 222, 2019.
2. Agar NS, Halliday GM, Barnetson RS, Ananthaswamy HN, Wheeler M and Jones AM: The basal layer in human squamous tumors harbors more UVA than UVB fingerprint mutations: A role for UVA in human skin carcinogenesis. Proc Natl Acad Sci USA 101: 4954-4959, 2004.
3. Battie C, Jitsukawa S, Bernerd F, Del Bino S, Marionnet C and Verschoore M: New insights in photoaging, UVA induced damage and skin types. Exp Dermatol 23: 7-12, 2014.
4. Ansary TM, Hossain MR, Kamiya K, Komine M and Ohtsuki M: Inflammatory molecules associated with ultraviolet radiation-mediated skin aging. Int J Mol Sci 22: 3974, 2021.
5. Elmets CA and Athar M: Milestones in photocarcinogenesis. J Invest Dermatol 133: E13-E17, 2013.
6. D'Orazio J, Jarrett S, Amaro-Ortiz A and Scott T: UV radiation and the skin. Int J Mol Sci 14: 12222-12248, 2013.
7. Brenner M and Hearing VJ: The protective role of melanin against UV damage in human skin. Photochem Photobiol 84: 539-549, 2008.
8. Fuller B: Role of PGE-2 and other inflammatory mediators in skin aging and their inhibition by topical natural anti-inflammatories. Cosmetics-Basel: 6, 2019.
9. de Jager TL, Cockrell AE and Du Plessis SS: Ultraviolet light induced generation of reactive oxygen species. Adv Exp Med Biol 996: 15-23, 2017.
10. Amaro-Ortiz A, Yan B and D'Orazio JA: Ultraviolet Radiation, Aging and the Skin: Prevention of damage by Topical cAMP manipulation. Molecules 19: 6202-6219, 2014.
11. Kammeyer A and Luiten RM: Oxidation events and skin aging. Ageing Res Rev 21: 16-29, 2015.
12. Tyrrell RM: Modulation of gene expression by the oxidative stress generated in human skin cells by UVA radiation and the restoration of redox homeostasis. Photoch Photobio Sci 11: 135-147, 2012.
13. Thiele JJ, Traber MG and Packer L: Depletion of human stratum corneum vitamin E: An early and sensitive in vivo marker of UV induced photo-oxidation. J Invest Dermatol 110: 756-761, 1998.
14. Cinat D, Coppes RP and Barazzuol L: DNA Damage-induced inflammatory microenvironment and adult stem cell response. Front Cell Dev Biol 9: 729136, 2021.
15. Tanveer MA, Rashid H and Tasduq SA: Molecular basis of skin photoaging and therapeutic interventions by plant-derived natural product ingredients: A comprehensive review. Heliyon 9: e13580, 2023.
16. Halicka HD, Huang X, Traganos F, King MA, Dai W and Darzynkiewicz Z: Histone H2AX phosphorylation after cell irradiation with UV-B-Relationship to cell cycle phase and induction of apoptosis. Cell Cycle 4: 339-345, 2005.
17. Revet I, Feeney L, Bruguera S, Segalés J, Díaz I, Galindo-Cardiel IJ, Martínez E, Darwich L, Fang Y, Maldonado J, *et al*: Functional relevance of the histone gammaH2Ax in the response to DNA damaging agents. Proc Natl Acad Sci USA 108: 8663-8667, 2011.
18. Georgoulis A, Vorgias CE, Chrousos GP and Rogakou EP: Genome instability and gammaH2AX. Int J Mol Sci 18: 1979, 2017.
19. Doyle LM and Wang MZ: Overview of extracellular vesicles, their origin, composition, purpose, and methods for exosome isolation and analysis. Cells-Basel 8: 727, 2019.
20. Zhang Y, Liu YF, Liu HY and Tang WH: Exosomes: Biogenesis, biologic function and clinical potential. Cell Biosci 9: 19, 2019.
21. Oh M, Lee J, Kim YJ, Rhee WJ and Park JH: Exosomes derived from human induced pluripotent stem cells ameliorate the aging of skin fibroblasts. Int J Mol Sci 19: 1715, 2018.
22. Choi JS, Cho WL, Choi YJ, Kim JD, Park HA, Kim SY, Park JH, Jo DG and Cho YW: Functional recovery in photo-damaged human dermal fibroblasts by human adipose-derived stem cell extracellular vesicles. J Extracell Vesicles 8: 1565885, 2019.
23. Tracy LE, Minasian RA and Caterson EJ: Extracellular matrix and dermal fibroblast function in the healing wound. Adv Wound Care 5: 119-136, 2016.
24. Shin JW, Kwon SH, Choi JY, Na JI, Huh CH, Choi HR and Park KC: Molecular mechanisms of dermal aging and antiaging approaches. Int J Mol Sci 20: 2126, 2019.
25. Greussing R, Hackl M, Charoentong P, Pauck A, Monteforte R, Cavinato M, Hofer E, Scheideler M, Neuhaus M, Micutkova L, *et al*: Identification of microRNA-mRNA functional interactions in UVB-induced senescence of human diploid fibroblasts. BMC Genomics 14: 224, 2013.
26. Najar M, Crompot E, van Grunsven LA, Dolle L and Lagneaux L: Foreskin-derived mesenchymal stromal cells with aldehyde dehydrogenase activity: Isolation and gene profiling. BMC Cell Biol 19: 4, 2018.

27. Badhani B, Sharma N and Kakkar R: Gallic acid: A versatile antioxidant with promising therapeutic and industrial applications. Rsc Adv 5: 27540-27557, 2015.
28. Livak KJ and Schmittgen TD: Analysis of relative gene expression data using real-time quantitative PCR and the 2(-Delta Delta C(T)) method. Methods 25: 402-408, 2001.
29. Ko MJ, Mulia GE and van Rijn RM: Commonly used Anesthesia/Euthanasia methods for brain collection differentially impact MAPK activity in male and female C57BL/6 Mice. Front Cell Neurosci 13: 96, 2019.
30. Boivin GP, Hickman DL, Creamer-Hente MA, Pritchett-Corning KR and Bratcher NA: Review of CO2 as a Euthanasia agent for laboratory rats and mice. J Am Assoc Lab Anim Sci 56: 491-499, 2017.
31. Kim YI, Kim KS, Ahn HJ, Kang IH and Shin MK: Reduced matrix metalloproteinase and collagen transcription mediated by the TGF-β/Smad pathway in passaged normal human dermal fibroblasts. J Cosmet Dermatol 19: 1211-1218, 2020.
32. Oh JH, Joo YH, Karadeniz F, Ko J and Kong CS: Syringaresinol inhibits UVA-induced MMP-1 expression by suppression of MAPK/AP-1 signaling in HaCaT keratinocytes and human dermal fibroblasts. Int J Mol Sci 21: 3981, 2020.
33. Kalluri R and LeBleu VS: The biology, function, and biomedical applications of exosomes. Science 367: eaau6977, 2020.
34. Shafei S, Khanmohammadi M, Heidari R, Ghanbari H, Taghdiri Nooshabadi V, Farzamfar S, Akbariqomi M, Sanikhani NS, Absalan M and Tavoosidana G: Exosome loaded alginate hydrogel promotes tissue regeneration in full-thickness skin wounds: An in vivo study. J Biomed Mater Res A 108: 545-556, 2020.
35. Wang C, Wang M, Xu T, Zhang X, Lin C, Gao W, Xu H, Lei B and Mao C: Engineering Bioactive Self-Healing antibacterial exosomes hydrogel for promoting chronic diabetic wound healing and complete skin regeneration. Theranostics 9: 65-76, 2019.
36. Fafian-Labora JA, Rodriguez-Navarro JA and O'Loghlen A: Small extracellular vesicles have GST activity and ameliorate senescence-related tissue damage. Cell Metab 32: 71-86.e5, 2020.
37. Han X, Wu P, Li L, Sahal HM, Ji C, Zhang J, Wang Y, Wang Q, Qian H, Shi H and Xu W: Exosomes derived from autologous dermal fibroblasts promote diabetic cutaneous wound healing through the Akt/β-catenin pathway. Cell Cycle 20: 616-629, 2021.
38. Gao W, Wang X, Si Y, Pang J, Liu H, Li S, Ding Q and Wang Y: Exosome derived from ADSCs attenuates ultraviolet B-mediated photoaging in human dermal fibroblasts. Photochem Photobiol 97: 795-804, 2021.
39. Ellistasari EY, Kariosentono H, Purwanto B, Wasita B, Riswiyant RCA, Pamungkasari EP and Soetrisno S: Exosomes derived from secretome human umbilical vein endothelial cells (Exo-HUVEC) Ameliorate the Photo-Aging of Skin Fibroblast. Clin Cosmet Inv Derm 15: 1583-1591, 2022.
40. Tanaka Y, Uchi H and Furue M: Antioxidant cinnamaldehyde attenuates UVB-induced photoaging. J Dermatol Sci 96: 151-158, 2019.
41. Wang L, Yang K, Jing R, Zhao W, Guo K, Hu Z, Liu G, Xu N, Zhao J, Lin L and Gao S: Protective effect of Saussurea involucrata polysaccharide against skin dryness induced by ultraviolet radiation. Front Pharmacol 14: 1089537, 2023.
42. Sandilands A, Sutherland C, Irvine AD and McLean WH: Filaggrin in the frontline: Role in skin barrier function and disease. J Cell Sci 122: 1285-1294, 2009.
43. Caricchio R, McPhie L and Cohen PL: Ultraviolet B radiation-induced cell death: Critical role of ultraviolet dose in inflammation and lupus autoantigen redistribution. J Immunol 171: 5778-5786, 2003.
44. Zhang M, An C, Gao Y, Leak RK, Chen J and Zhang F: Emerging roles of Nrf2 and phase II antioxidant enzymes in neuroprotection. Prog Neurobiol 100: 30-47, 2013.
45. Angelis KJ, Zaveska Drabkova L, Vagnerova R and Hola M: RAD51 and RAD51B play diverse roles in the repair of DNA double strand breaks in physcomitrium patens. Genes (Basel) 14: 305, 2023.
46. Deng M, Xu Y, Yu Z, Wang X, Cai Y, Zheng H, Li W and Zhang W: Protective effect of fat extract on UVB-Induced photoaging in vitro and in vivo. Oxid Med Cell Longev 2019: 6146942, 2019.
47. Granados-Lopez AJ, Manzanares-Acuña E, López-Hernández Y, Castañeda-Delgado JE, Fraire-Soto I, Reyes-Estrada CA, Gutiérrez-Hernández R and López JA: UVB Inhibits proliferation, cell cycle and induces apoptosis via p53, E2F1 and microtubules system in cervical cancer cell lines. Int J Mol Sci 22: 5197, 2021.
48. Tewari M, Quan LT, Orourke K, Desnoyers S, Zeng Z, Beidler DR, Poirier GG, Salvesen GS and Dixit VM: Yama/CPP32 beta, a mammalian homolog of CED-3, is a CrmA-inhibitable protease that cleaves the death substrate poly(ADP-ribose) polymerase. Cell 81: 801-809, 1995.
49. Henninger HB, Ellis BJ, Scott SA and Weiss JA: Contributions of elastic fibers, collagen, and extracellular matrix to the multiaxial mechanics of ligament. J Mech Behav Biomed 99: 118-126, 2019.
50. Varani J, Spearman D, Perone P, Fligiel SE, Datta SC, Wang ZQ, Shao Y, Kang S, Fisher GJ and Voorhees JJ: Inhibition of type I procollagen synthesis by damaged collagen in photoaged skin and by collagenase-degraded collagen in vitro. Am J Pathol 158: 931-942, 2001.